Large Voltage-Induced Changes in the Perpendicular Magnetic Anisotropy of an MgO-Based Tunnel Junction with an Ultrathin Fe Layer

Takayuki Nozaki,[1,*] Anna Kozioł-Rachwał,[1,2] Witold Skowroński,[1,3] Vadym Zayets,[1] Yoichi Shiota,[1] Shingo Tamaru,[1] Hitoshi Kubota,[1] Akio Fukushima,[1] Shinji Yuasa,[1] and Yoshishige Suzuki[1,4]

[1]*National Institute of Advanced Industrial Science and Technology, Spintronics Research Center, Tsukuba, Ibaraki 305-8568, Japan*

[2]*AGH University of Science and Technology, Faculty of Physics and Applied Computer Science, Al. Mickiewicza 30, 30-059 Kraków, Poland*

[3]*AGH University of Science and Technology, Department of Electronics, Al. Mickiewicza 30, 30-059 Kraków, Poland*

[4]*Graduate School of Engineering Science, Osaka University, 1-3 Machikaneyama, Toyonaka, Osaka 560-8531, Japan*

(Received 17 September 2015; revised manuscript received 27 January 2016; published 15 April 2016)

We study the voltage control of perpendicular magnetic anisotropy in an ultrathin Fe layer sandwiched between the Cr buffer and MgO tunneling barrier layers. A high-interface magnetic anisotropy energy of $2.1\ \mathrm{mJ/m^2}$ is achieved in the Cr/ultrathin Fe/MgO structure. A large voltage-induced perpendicular magnetic anisotropy change is observed under the negative-bias voltage applications for the case of the Fe layer thinner than 0.6 nm. The amplitude of the voltage-induced anisotropy energy change exhibits a strong Fe-thickness dependence and it reaches as high as 290 fJ/Vm. The observed high values of the surface anisotropy and voltage-induced anisotropy energy change demonstrate the feasibility of voltage-driven spintronic devices.

DOI: 10.1103/PhysRevApplied.5.044006

I. INTRODUCTION

Voltage control of magnetic anisotropy (VCMA) in ferromagnetic metal films is a promising technology for the low-power manipulation of spin [1–22]. Because of screening by free electrons, the penetration of the electric field into a metal is limited to the surface, unlike in the case of a semiconductor [23]; therefore, the realization of the VCMA effect has long been considered to be impractical. However, very recently, the VCMA effect has been demonstrated in an all-solid-state device using an ultrathin $3d$ transition ferromagnetic metal with a thickness of the order of a few atomic layers [2]. The demonstration of a substantial voltage-induced anisotropy change in an MgO-based magnetic tunnel junction (MTJ) [10,11] produced a great impact. It has led to the demonstration of voltage-induced ferromagnetic resonance excitation [24,25] and dynamic magnetization switching driven solely by the application of a voltage [26,27] or with the additional assistance of the spin-transfer torque [28,29]. This progress shows the feasibility of voltage-based spintronic devices, such as voltage-torque magnetic random access memory (MRAM).

Several possible physical origins of the VCMA effect have been discussed. A charge accumulation at a metal-barrier interface is the most probable reason of the VCMA effect. The charge accumulation or depletion may affect the spin-dependent screening at the interface [30], resulting in the change in band structure [31] and the electronic occupancy of $3d$ orbitals [32]. The charge accumulation or depletion can induce the perpendicular magnetic anisotropy (PMA), because of the modification of the spin-orbit interaction at an interface. Recently, other possible origins, such as the voltage-induced redox reaction [33,34], the electromigration [14], the piezoelectric effect [19], and the Rashba effect [35,36] are also being discussed. Actually, simultaneous contributions to the VCMA effect should be considered. For memory applications, the VCMA effect should be fast with high writing endurance. The redox reaction, the electromigration, or the charge-trapping effects in dielectric materials can cause a substantial VCMA effect of a few thousands of fJ/Vm [14,33,37]. However, even if improvements are possible, the limit of operating speed and the writing endurance in these cases are still under discussion. In contrast, the VCMA due to the modulation of the charge accumulation without charge trapping can be fast. The subnanosecond modulation of the VCMA effect was already demonstrated [24–27]. Unfortunately, the presently achieved magnitude of this type of the VCMA effect is only 100 fJ/Vm [17,21]. Therefore, for practical applications, it is important to develop materials with a higher magnitude of the charge-accumulation-based VCMA effect.

The scalability of the VCMA effect is another critical issue for practical applications. A larger VCMA effect is required for smaller-size magnetic elements. This

*nozaki-t@aist.go.jp

 © 2016 American Physical Society

requirement can be understood as follows. In order to maintain sufficient thermal stability, a larger PMA is required for a smaller-size magnetic element. In order to store data in a magnetic element, its PMA energy should substantially exceed the energy of the thermal fluctuations. For example, for a gigabit-class MRAM with the cell size smaller than 30 nm Φ, the $E_{\mathrm{perp}}t_{\mathrm{free}}$ value should be in the range of 0.4–0.6 $\mathrm{mJ/m^2}$, where E_{perp} is the PMA energy and t_{free} is the free-layer thickness [38]. Since a substantial VCMA effect may occur only in an ultrathin film, the film should have a sufficiently large energy of the PMA. In order to reverse the magnetization by a voltage in a film with a larger PMA, the VCMA should be larger as well. In the case of the dynamic switching, the accurate magnetization switching can occur when the direction of the total magnetic anisotropy changes from the perpendicular-to-plane direction to the in-plane direction, or vice versa [26,27]. It literally means that the VCMA effect needs to exceed the intrinsic PMA during the switching with an additional external bias magnetic field, which is required to exert the voltage-induced torque on magnetization effectively, and also determine the switching speed. For example, in order to reverse the magnetization of a film having a PMA of 0.4–0.6 $\mathrm{mJ/m^2}$ and 1–1.4 $\mathrm{mJ/m^2}$, which correspond to the technology node of 30 nmΦ and 20 nmΦ for MRAM [38], the VCMA should exceed 400–600 fJ/Vm and $1000-1400$ fJ/Vm under the assumption of an applicable electric field of 1 V/nm. The large VCMA effect is also very important to achieving a low writing-error rate of the dynamic magnetization switching [39]. It can be effective not only for the dynamic switching, but also even when we use it to assist the external magnetic-field-induced [3,17] or spin-transfer torque-induced switching [28], although the PMA is not required to be fully nulled out in these cases. However, as was mentioned above, the charge-accumulation-based VCMA effect is limited to be 100 fJ/Vm at present, therefore, it is not sufficient for these targets.

One of the promising structures, which might have the required large PMA and VCMA effect, is a Cr/ultrathin Fe/MgO structure. The large interface anisotropy [40,41] and the suppression of the surface segregation [42] are the reasons why the large PMA and VCMA effect might be expected for this structure.

In this work, we investigate the PMA and the VCMA effect in an ultrathin Fe layer sandwiched between a Cr buffer and an MgO barrier layer. We observe the VCMA effect as high as 290 fJ/Vm and the high-interface anisotropy energy $K_{i,0}$ of 2.1 $\mathrm{mJ/m^2}$. In the case of the Fe layer thinner than 0.6 nm, a linear increase in the PMA is observed when a negative bias voltage is applied. In contrast, PMA change deviates from the linear relation under a positive bias voltage. In addition, the amplitude of the VCMA effect depends strongly on the Fe thickness, which cannot be expected from the simple model of a carrier-mediated effect on the surface anisotropy. The demonstration of the large VCMA effect in the Fe/MgO junction offers a path to developing future voltage-driven spintronic devices.

II. EXPERIMENT

Figure 1 shows a schematic diagram of the MTJ used in this study. A fully epitaxial multilayer comprising an MgO seed (3 nm)/Cr buffer (30 nm)/ultrathin Fe ($t_{\mathrm{Fe}} = 0.3-1.0$ nm)/MgO (2.3 nm)/Fe (10 nm)/Ta/Ru is deposited on a MgO(001) single-crystal substrate by molecular beam epitaxy. Here, the bottom ultrathin Fe film is the voltage-driven free layer with perpendicular magnetization and the top 10-nm-thick Fe layer is the reference layer with in-plane magnetization. The MgO (001) seed and Cr (001) buffer layers are deposited at 200 °C followed by annealing at 800 °C. This postannealing process under the high temperature is crucial to obtaining the flat Cr buffer and even the high PMA in the ultrathin Fe layer [41]. The ultrathin Fe-free layer is grown at a substrate temperature of 200 °C and annealed at 260 °C. Then, after cooling the substrate temperature to 70 °C, a 2.3-nm-thick MgO(001) barrier layer is deposited and annealed at 350 °C for the high PMA at the Fe/MgO interface. The perpendicularly magnetized Fe layer is obtained even annealed under higher temperatures, however, the Fe-thickness dependence of PMA became scattering as observed in the previous study [41], probably because of the heavy intermixing at the Cr/Fe interface. Finally, the 10-nm-thick Fe reference layer is deposited at 260 °C and the multilayer is covered by a sputter-deposited Ta/Ru capping layer. The film is patterned into squares

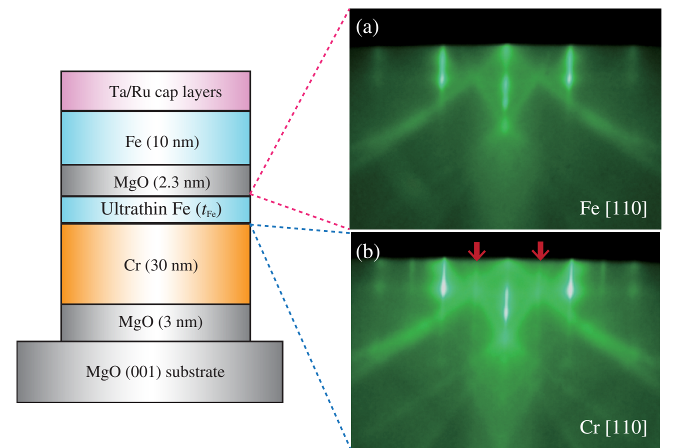

FIG. 1. Schematic illustration of epitaxial magnetic tunnel junctions with an ultrathin Fe layer sandwiched between the Cr buffer and MgO barrier layers, and RHEED patterns for the surface of (a) an ultrathin Fe (0.8 nm) layer and (b) a Cr buffer layer. The incident electron beam is along the Fe[110] and Cr[110] azimuths. Weak half-order streaks are observed only for the Cr surface (red arrows).

with areas of $2 \times 6\ \mu\text{m}^2$ using the optical lithography, ion-beam milling, and lift-off processes. The tunneling magnetoresistance (TMR) is measured using a conventional direct current two-probe method under in-plane external magnetic fields (H_{ex}) at room temperature. The polarity of the bias voltage is defined with respect to the top Fe electrode. The resistance-area (RA) product of the MTJs is about $60\ \text{k}\Omega\,\mu\text{m}^2$. Because of the high RA value, the highest used current density is below $2 \times 10^3\ \text{A/cm}^2$.

III. STRUCTURAL ANALYSIS AND MAGNETIC PROPERTIES

The reflection high-energy electron diffraction (RHEED) patterns for the ultrathin Fe (0.8 nm) and Cr buffer layers are shown in Figs. 1(a) and 1(b), respectively. The incident electron beam is parallel to the [110] azimuths of the Cr and Fe layers. As is observed in the previous work [41], the half-order streaks, which indicate the formation of a (2×2) reconstructed surface, are observed in the Cr buffer layer [red arrows in Fig. 1(b)]. However, there is no reconstruction on the surface of the ultrathin Fe layer. The (2×2) surface reconstruction can be related either to the presence of carbon [43] or oxygen [41] impurities on the Cr(001) surface. To clarify the origin of the observed surface reconstructions, we performed *in situ* Auger electron spectroscopy under a primary voltage of 5 kV for the surfaces of the Cr and ultrathin Fe (0.6 nm) as shown in Fig. 2. A clear signal from carbon (C) is seen at a kinetic energy of 275 eV. However, the signal from the oxygen, which should be at 510 eV, is not observed. It indicates that the surface reconstruction of the Cr buffer layer is attributed to the carbon, which can be segregated during the high-temperature annealing of the buffer layer. We observe a small signal from carbon even at the surface of the ultrathin Fe layer, although its intensity is strongly attenuated. It is difficult to distinguish whether the signal comes from the surface of the Fe layer or from the Cr buffer layer. Because the escape depth of the Auger electrons can be a few nanometers in our measurements, therefore, we might detect signals from both the ultrathin Fe and Cr buffer layers. However, it should be emphasized that the ratio of the C/Cr signal intensities is almost the same in both cases, about 0.16 for the Cr surface and 0.14 for the Fe surface. If most of the carbon atoms segregate on the Fe surface, the C/Cr ratio should increase. Therefore, these results imply that the carbon contamination mainly exists in the Cr buffer layer, as expected from the RHEED observation.

Next, we discuss the property of perpendicular magnetic anisotropy from TMR curves. In this discussion, we take into account the existence of a magnetic dead layer with thickness t_d of 0.1 nm, and use the actual thickness, $t'_{\text{Fe}} = t_{\text{Fe}} - t_d$. The t_d value is evaluated from the Fe-thickness dependence of the magnetic moment per area [see the inset in Fig. 3(c)]. The magnetic moment is measured by the superconducting quantum interference device (SQUID).

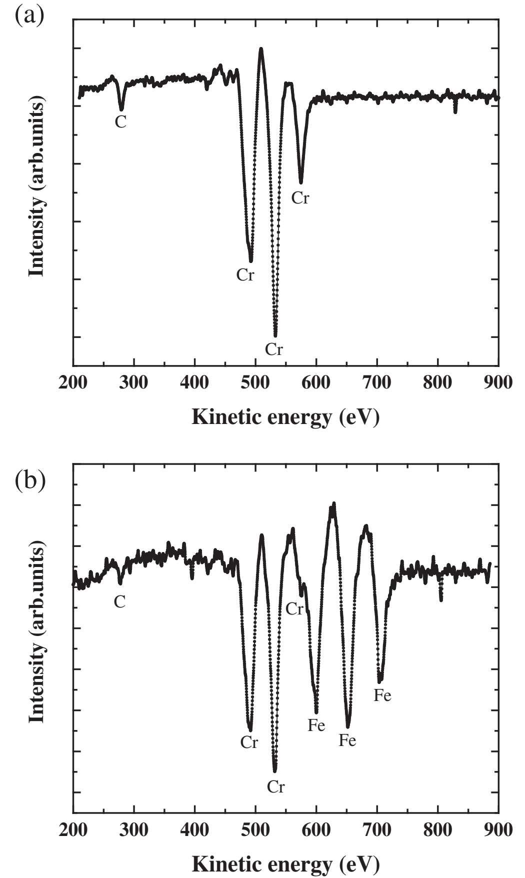

FIG. 2. Auger spectra obtained at the surface of (a) the Cr buffer and (b) 0.6-nm-thick Fe layers.

Figure 3(a) shows an example of the full MR loop measured under the in-plane magnetic field application for the sample with $t'_{\text{Fe}} = 0.47$ nm. Because of a high-interface anisotropy and a thin thickness, the magnetic easy axis of the ultrathin Fe layer is perpendicular to the film plane. In contrast, the magnetization of the top reference Fe layer is in plane, because of the demagnetization field. Therefore, two magnetizations are orthogonal under zero magnetic field. Application of an in-plane magnetic field tilts the magnetization of the ultrathin Fe layer into the direction of its magnetic hard axis. As a result of the rotation of the free layer's magnetization towards the sample plane, we observe a gradual reduction in the tunneling resistance with a peak at zero magnetic field [see the drawings in Fig. 3(a)]. Since the coercivity of the in-plane magnetized reference layer is small enough (<100 Oe), it has almost no influence on the TMR curve. In the case of an out-of-plane applied magnetic field, the magnetization of only the Fe reference layer gradually tilts toward the perpendicular direction, so that the tunneling resistance varies linearly with the magnetic field. In addition, the existence of the PMA is confirmed by observing a sharp switching of the ultrathin Fe layer in the

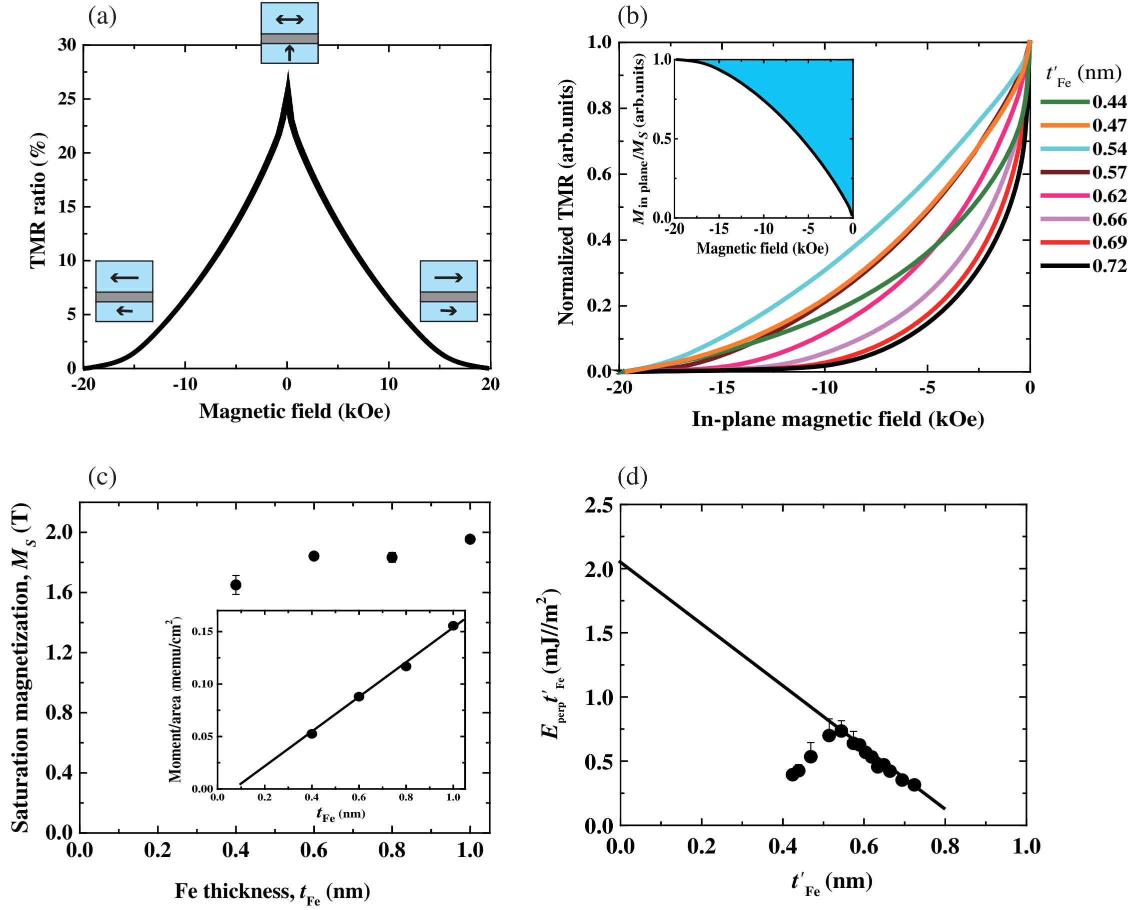

FIG. 3 (a) Full TMR curve for the MTJ with $t'_{Fe} = 0.47$ nm measured under in-plane magnetic fields, (b) The normalized TMR curves as a function of applied in-plane magnetic field measured for different Fe thicknesses. The inset shows the in-plane component of the magnetization of the ultrathin Fe layer ($t'_{Fe} = 0.57$ nm) versus the applied in-plane magnetic fields. The PMA energy is estimated by calculating the area of the blue-colored part (see text). (c) Fe-thickness dependence of saturation magnetization value M_S obtained from SQUID measurement. The inset shows the Fe-thickness dependence of the magnetic moment per area for the evaluation of magnetic dead layer thickness t_d. (d) The product of the energy of the perpendicular magnetic anisotropy E_{perp} and the Fe thickness t'_{Fe} as the function of t'_{Fe}.

out-of-plane direction in the case of the perpendicularly magnetized MTJs (not shown here).

Figure 3(b) shows the t'_{Fe} dependence of the normalized TMR curves. Here, we focus only on the negative magnetic field ranges in order to show the differences clearly. Clear shifts in the saturation field are observed due to the change in the interface-induced PMA.

The PMA of the ultrathin Fe layer are evaluated from the measured TMR curves as follows. The tunneling conductance G depends on the relative angle (θ) between the magnetizations of the ultrathin and reference Fe layers, i.e., $G(\theta) = G_{90} + (G_P - G_{90})\cos\theta$. Here, G_{90} and G_P is the conductance under the orthogonal and parallel magnetization configurations. In the case of an in-plane magnetic field, it could be assumed that the magnetization of the Fe reference layer always lies in the film plane. Therefore, for the ultrathin Fe layer, the ratio of its in-plane component of the magnetization $M_{\text{in plane}}$ to its saturation magnetization M_S can be calculated as

$$\frac{M_{\text{in plane}}}{M_S} = \cos\theta = \frac{R_{90} - R(\theta)}{R(\theta)} \frac{R_P}{R_{90} - R_P}, \quad (1)$$

where R_P is the MTJ resistance in the case of parallel magnetizations measured under the $H_{ex} = 20$ kOe, R_{90} is the MTJ resistance in the case of the orthogonal measured under the zero magnetic field, and $R(\theta)$ is the MTJ resistance in the case when the magnetization of the Fe ultrathin layer is tilted towards the in-plane direction at angle θ under an applied in-plane magnetic field. From Eq. (1), it is possible to evaluate the normalized in-plane magnetization versus an applied magnetic field (normalized M-H curve). The inset graph in Fig. 3(b) shows an example of the normalized M-H curve obtained from the TMR curve for the MTJ with $t'_{Fe} = 0.57$ nm under the bias voltage of 10 mV. Finally, the PMA energy density E_{perp} can be evaluated by calculating the $M_{\text{in plane}}$ (H) area [see the blue area in the inset of Fig. 3(b)] with the saturation

magnetization value evaluated from the SQUID measurements.

E_{perp} can be expressed by the phenomenological expression [44] $E_{perp} = K_{i,0}/t'_{Fe} + K_V$, where $K_{i,0}$ is an interface anisotropy energy and K_V is the volume anisotropy. This equation means that the anisotropy energy induced by the interface effect can be evaluated from the plot of $E_{perp}t'_{Fe}$ as a function of t'_{Fe} as an intercept at $t'_{Fe} = 0$. Figure 3(d) shows the dependence of $E_{perp}t'_{Fe}$ on the Fe thickness t'_{Fe}. The expected linear relationship between $E_{perp}t'_{Fe}$ and t'_{Fe} is observed for $t'_{Fe} > 0.55$ nm and the $K_{i,0}$ is estimated to be (2.1 ± 0.1) mJ/m^2. This value is comparable to the previously reported one [41]. In the case of Ref. [41], the $K_{i,0}$ is evaluated from the E_{perp} under the fixed Fe thickness with the K_V value expected from the saturation magnetization. On the other hand, we could confirm a systematic Fe-thickness dependence in the thicker Fe-thickness ranges. It should be noted that the large PMA is not observed in a Cr/Fe/Cr sandwich structure. For example, in the case of a Cr/Fe ($t'_{Fe} = 0.5$ nm)/Cr structure, a high perpendicular field of about 15 kOe is required to saturate the magnetization in the out-of-plane direction (not shown here). Therefore, the high positive interface anisotropy observed in our studies is related to the Fe/MgO interface. The first-principle calculations support these results and predict that a large interface anisotropy is attributed to the hybridization of Fe-d_{z2} and O-p_z orbitals at the Fe/MgO interface [45–47].

$E_{perp}t'_{Fe}$ versus t'_{Fe} deviates from the linear behavior for $t'_{Fe} < 0.55$ nm. There exist several possible origins relating to this behavior. For example, a reduction in the Curie temperature due to the limited range of spin-spin interactions [48] is often discussed, however, we confirm that the saturation magnetization value took almost a constant value between 100 and 350 K, even at $t'_{Fe} < 0.5$ nm (not shown here). Therefore, the observed deviation probably originates from other influences, such as the magnetoelastic effect [49], and an intermixing at the Cr/Fe interface, which is evidenced by the finite magnetic dead layer and lowered M_S value compared with that of bulk (2.2 T) as shown in Fig. 3(c). These effects can be influential, especially in the ultrathin Fe-thickness region. Additionally, carbon contamination at the Fe/MgO interface can also be responsible. According to the AES and RHEED studies, we conclude that segregated carbon exists mainly at the Cr/Fe interface. However, we cannot yet deny the possibility of a small amount of contamination even at the Fe/MgO interface, especially in the ultrathin Fe-thickness region. For example, we observe a monotonic increase in the coercivity of the perpendicularly magnetized Fe layer ($t'_{Fe} = 0.4$ nm) when the thickness of the MgO seed layer is increased from 0 to 3 nm (not shown here). These studies show evidence that finite carbon contamination can exist at the Fe/MgO interface and its presence might be crucial for magnetic anisotropy.

IV. VOLTAGE CONTROL OF MAGNETIC ANISOTROPY

To examine the VCMA effect in the ultrathin Fe layer, the bias voltage dependence of the TMR curves is studied. Since both the tunneling resistance and the TMR ratio strongly depend on the bias voltage, the TMR curves are normalized using the maximum ($H_{ex} = 0$ Oe) and minimum ($H_{ex} = 20$ kOe) resistances. After the normalizing process, influences from the bias voltage dependence of tunneling resistance and MR ratio can be excluded; therefore, we can focus only on the VCMA effect. Figure 4 shows the normalized TMR curves [(a)–(c)] and normalized M-H curves [(d)–(f)] measured at different bias voltages for the case of (a),(d) $t'_{Fe} = 0.44$ nm; (b),(e) 0.57 nm; and (c),(f) 0.69 nm, respectively. The applied bias voltage range of $V_b = \pm 800$ mV corresponds to the electric-field range of $E = V_b/t_{MgO} = \pm 350$ mV/nm. We observe a clear dependence of the normalized TMR curves on the applied voltage, indicating a substantial VCMA effect in the ultrathin Fe layer. The dependence is more pronounced for the case of a thinner Fe layer. The PMA energy under each bias voltage condition is evaluated by the same method, which is described above. The bias voltage dependence of $E_{perp}t'_{Fe}$ as a function of the applied electric field is summarized in Fig. 4 for (g) $t'_{Fe} = 0.44$ nm, (h) 0.57 nm, and (i) 0.69 nm, respectively. For the case of $t'_{Fe} = 0.69$ nm, the $E_{perp}t'_{Fe}$ depends on the applied electric field almost linearly with the small additional quadratic term. The slope of the linear term is evaluated to be about 80 fJ/Vm. The linear dependence is also observed for an Fe alloy/MgO junction in previous works [10,11,17]. A possible reason for the dependence of the VCMA effect on the voltage polarity is that the VCMA effect might depend on whether the electrons are accumulated or depleted at the Fe/MgO interface, and the electron depletion generally causes the PMA enhancement. Here, it should be emphasized that the observed effect cannot be explained by an influence of spin-transfer torque (STT). The STT effect can be more effective with the assistance of the VCMA effect, even though the flowing current density is much smaller than the critical current density for STT switching [28]. However, in our experimental configuration, for example, STT under the negative bias voltage prefers the parallel magnetization configuration, which should cause the reduction in the saturation field. This trend is the opposite of that observed in this study.

Interestingly, for the thinner ranges, we observe a characteristic behavior in the anisotropy plot. $E_{perp}t'_{Fe}$ exhibits a linear increase in the negative bias direction. On the other hand, unexpectedly, the PMA change deviates from the linear relation under $E > +90$ mV/nm and takes an almost constant value [see Figs. 4(g) and 4(h)].

Since the VCMA effect is linearly proportional to the applied voltage in the wide range, the slope of this

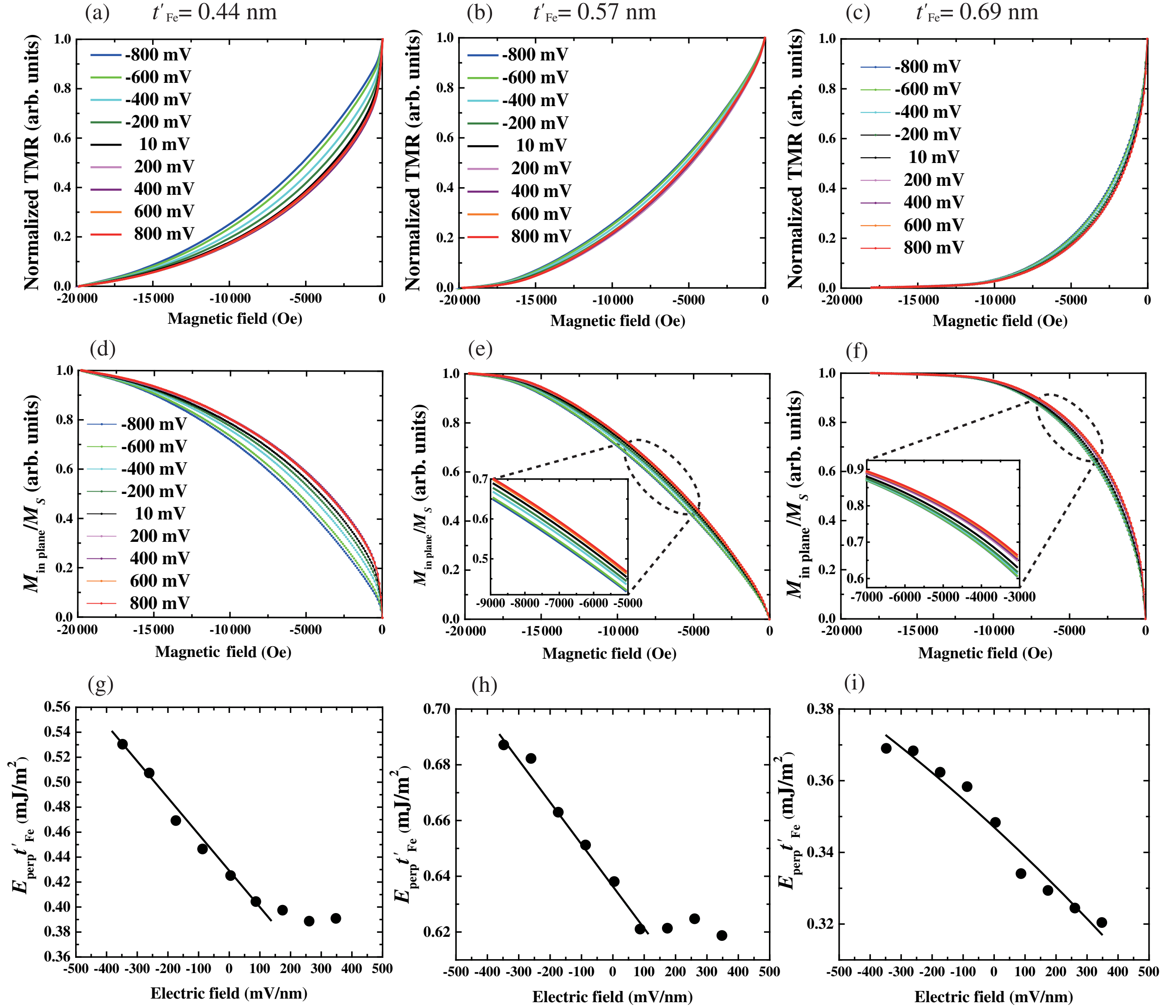

FIG. 4. The normalized TMR curves [(a)–(c)], normalized *M*-*H* curves [(d)–(f)] obtained under different bias voltage conditions, and the summary of estimated $E_{\mathrm{perp}}t'_{\mathrm{Fe}}$ as the function of applied electric fields [(g)–(i)] with different Fe thicknesses of (a),(d),(g) $t'_{\mathrm{Fe}} = 0.44$ nm; (b),(e),(h) $t'_{\mathrm{Fe}} = 0.57$ nm; (c),(f),(i) $t'_{\mathrm{Fe}} = 0.69$ nm, respectively.

proportionality can be used to characterize the magnitude of the VCMA effect. We define this slope as the VCMA coefficient. Figure 5 shows the VCMA coefficient as a function of Fe thickness t'_{Fe}. For the samples with $t'_{\mathrm{Fe}} < 0.6$ nm, the VCMA coefficient is evaluated in the electric-field range between -350 and 90 mV/nm. Unexpectedly, there is a significant dependence of the VCMA coefficient on the thickness of the Fe layer. It could be assumed that the magnitude of the VCMA effect is linearly proportional to the charge accumulation at the Fe/MgO interface. The classical model of conductivity in metal limits the size of a charge accumulation to an infinitely thin region at a metal-dielectric interface. It means that at any thickness of the Fe, the charge accumulation should be limited only at the interface and the magnitude of the VCMA effect should not depend on the Fe thickness. Contrary to the above expectation, the VCMA coefficient shows a clear increase for $t'_{\mathrm{Fe}} < 0.6$ nm and it reaches as high as 290 fJ/Vm with the PMA of about $E_{\mathrm{perp}}t'_{\mathrm{Fe}} > 0.5$ mJ/m^2. For the application purpose of voltage-induced dynamic switching or voltage-assisted STT switching, controllability of reduction in the PMA is desired, while we observe only the enhancement of the PMA in this study. However, such properties can be useful for other purposes, such as domain-wall devices [50,51] or spin-orbit-torque devices [52].

In the following, we discuss the possible origin of the large VCMA effect observed only under the negative bias direction and the unexpected Fe-thickness dependence. For example, the voltage-driven redox effect, e.g.,

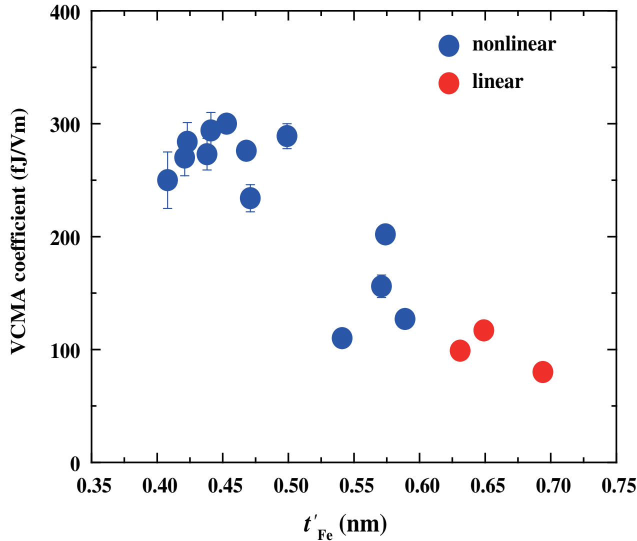

FIG. 5. The VCMA coefficient as a function of the Fe thickness. The nonlinear bias voltage dependence is observed for the Fe layers thinner than 0.6 nm (blue dots) and the linear dependence is observed for the thicker Fe layers (red dots).

voltage-driven oxygen ion migration into an ultrathin ferromagnetic metal layer [33], can cause a nonlinear reduction in the PMA through the oxidation process. A negatively charged ion of oxygen may diffuse from the MgO towards the Fe layer under a negative bias (as for the polarity of the bias defined in our experiment). The diffusion of the oxygen ion into the Fe layer should assist the formation of a Fe oxide. As a consequence, in the case of a negative bias the PMA should be reduced. In our experiment, we observe a clear enhancement in the PMA for a negative bias. It indicates that the contribution of the redox effect can be excluded.

Other possibilities we have to consider are influences of electromigration and/or charge-trapping effects in the MgO barrier. For example, misfit dislocations in the MgO thin film can act as charge-trapping sites [53]. One characteristic feature of these effects is the delay and/or the hysteretic behavior of the VCMA effect under the voltage-sweep measurement. A similar large VCMA effect with nonlinear voltage dependence is observed in a V/ultrathin Fe/MgO/Fe junction [14], although the sign of the VCMA effect is opposite to our results, i.e., the electric field, which causes the electron depletion, resulted in the decrease of the PMA in the case of Ref. [14]. The electromigration or the charge-trapping effect in the MgO barrier are suggested as the origin, because a very long transient time is required to saturate the PMA change. To confirm this property in our samples, we perform cyclic measurements of the VCMA effect for the MTJ with $t'_{Fe} = 0.45$ nm as summarized in Fig. 6. TMR curves are measured under each bias condition taking 2 min per loop. The yellow area shows the initial sweep, which is the first of the TMR measurements after the sample fabrication.

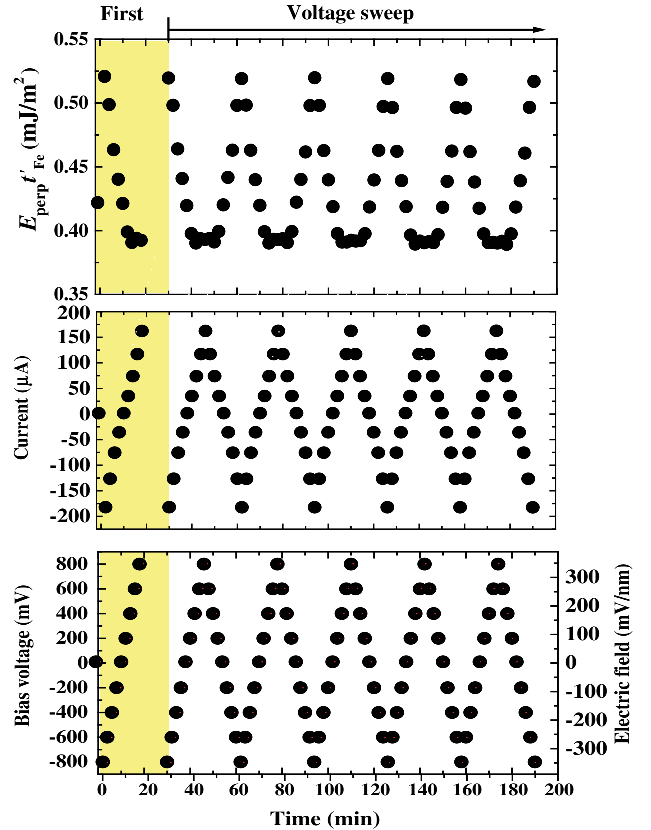

FIG. 6. Cyclic measurements of the VCMA effect for the MTJ with $t'_{Fe} = 0.45$ nm. The yellow area shows the result of the measurement when the voltage is applied to the MTJ for the first time after the MTJ fabrication. The applied bias voltages are swept back and forth between $V_b = -800$ mV and 800 mV 10 times and the value of $E_{perp}t'_{Fe}$ is evaluated at each bias condition.

Then, the bias voltage is swept back and forth between $V_b = -800$ mV and 800 mV ten times and the $E_{perp}t'_{Fe}$ value is evaluated under each bias condition. The nonlinear change in the PMA is well reproduced and neither delay nor hysteretic behavior are observed, at least in the time scale of a few minutes. These results imply that the observed effect does not relate to the high density of defects in the dielectric material as observed in previous works [14,37]. On the other hand, a very fast charge-trapping and detrapping process has been observed even in the thin MgO barrier in the time scale of the order of 100 ns [54], through much lower density of charge-trapping sites. Therefore, our demonstrations are not yet enough to completely rule out the possibility of charge trapping or small atomic displacement effects in the MgO barrier. We need to make clear how large those effects can occur in the single-crystal MgO barrier and if they can interpret the observed large VCMA effect or not. Further high-speed experimentation, for example, using the electric-field-induced ferromagnetic resonance [24,25] is also required. In addition, it is important to confirm that we have no chemical reaction at the Fe/MgO interface, for example, by

using the XMCD measurement under the electric-field application [55].

The existence of the piezoelectric effect in the MgO barrier has been confirmed recently by the piezoresponse force microscopy [19]. The piezoelectric effect can be a possible reason for the unexpected Fe-thickness dependence of the VCMA effect. However, the reported piezoelectric effect is symmetrical with respect to the voltage polarity. On the other hand, the large VCMA effect is observed only in the negative bias direction in our experiment, therefore, the piezoelectric contribution looks unlikely as the origin of the observed VCMA effect at present.

Another intriguing possible origin of the deviation from the linearity is an influence of interface resonance states in the Fe layer. It is well known that localized surface states are formed at the Fe/MgO interface [56]. The first principle calculations predict that the localized surface states may act as intrinsic charge-trapping sites and make the reverse point of the VCMA effect [57]. The VCMA contribution due to the localized surface states may change its polarity depending on the energy of the localized states. It should be noted that the probability of the scattering of an electron from a localized surface state into a delocalized state of the conduction electrons is high. Therefore, any delay of the VCMA response or a hysteretic behavior should not be expected due to the charge capture on the localized surface states.

In addition, an influence of Fe and Cr intermixing on the VCMA effect should be considered [58,59]. The intermixing at the Cr/Fe interface may occur during the deposition and postannealing process at high temperature. In our experiment, a notable nonlinear behavior is observed for $t'_{\mathrm{Fe}} < 0.6$ nm. Interestingly, the deviation from the linear relation in the $E_{\mathrm{perp}} t'_{\mathrm{Fe}}$ also occurred at around the same thickness. In the case of such a thin layer, partial alloying or even the existence of a Cr layer, which can couple with Fe atoms antiferromagnetically, close to the Fe/MgO interface should affect the electronic structure chemically and/or elastically [60]. Consequently, it may result in an unexpected Fe-thickness dependence of the PMA and the VCMA effects. Systematic investigation by first-principles calculations would be helpful to make the origin of the observed behavior clear.

V. CONCLUSION

In summary, we investigate the voltage-induced magnetic anisotropy change in an ultrathin Fe layer sandwiched between the Cr buffer and MgO barrier layers. A high-interface anisotropy energy of 2.1 $\mathrm{mJ/m^2}$ is demonstrated at the Fe/MgO interface. We observe the large VCMA effect under the negative bias voltage applications for the case of the Fe layer thinner than 0.6 nm. The VCMA coefficient increases with decreasing the Fe thickness and it reaches as high as 290 fJ/Vm. This large voltage effect in an Fe/MgO junction demonstrates the feasibility of a class of voltage-controlled spintronic devices, which could be competitive with the present spin-transfer-torque devices.

ACKNOWLEDGMENTS

We thank K. Nakamura, T. Oda, M. Tsujikawa, M. Shirai, and J. Ieda for fruitful discussions and E. Usuda for assistance with the experiments. This work was partly supported by the ImPACT Program of the Council for Science, Technology and Innovation, the Strategic AIST integrated R&D program “IMPULSE,” and a Grant-in-Aid for Scientific Research (No. 26709046).

[1] M. Weisheit, S. Fähler, A. Marty, Y. Souche, C. Poinsignon, and D. Givord, Electric field-induced modification of magnetism in thin-film ferromagnets, Science **315**, 349 (2007).

[2] T. Maruyama, Y. Shiota, T. Nozaki, K. Ohta, N. Toda, M. Mizuguchi, A. A. Turapurkar, T. Shinjo, M. Shiraishi, S. Mizukami, Y. Ando, and Y. Suzuki, Large voltage-induced magnetic anisotropy change in a few atomic layers of iron, Nat. Nanotechnol. **4**, 158 (2009).

[3] Y. Shiota, T. Maruyama, T. Nozaki, T. Shinjo, M. Shiraishi, and Y. Suzuki, Voltage-assisted magnetization switching in ultrathin $\mathrm{Fe_{80}Co_{20}}$ alloy layers, Appl. Phys. Express **2**, 063001 (2009).

[4] S.-S. Ha, N.-H. Kim, S. Lee, C.-Y. You, Y. Shiota, T. Maruyama, T. Nozaki, and Y. Suzuki, Voltage induced magnetic anisotropy change in ultrathin $\mathrm{Fe_{80}Co_{20}}$/MgO junctions with Brillouin light scattering, Appl. Phys. Lett. **96**, 142512 (2010).

[5] T. Zhou, S. H. Leong, Z. M. Yuan, S. B. Hu, C. L. Ong, and B. Liu, Manipulation of magnetism by electrical field in a real recording system, Appl. Phys. Lett. **96**, 012506 (2010).

[6] M. Endo, S. Kanai, S. Ikeda, F. Matsukura, and H. Ohno, Electric-field effects on thickness dependent magnetic anisotropy of sputtered $\mathrm{MgO/Co_{40}Fe_{40}B_{20}}$/Ta structures, Appl. Phys. Lett. **96**, 212503 (2010).

[7] F. Bonell, S. Murakami, Y. Shiota, T. Nozaki, T. Shinjo, and Y. Suzuki, Large change in perpendicular magnetic anisotropy induced by an electric field in FePd ultrathin films, Appl. Phys. Lett. **98**, 232510 (2011).

[8] T. Seki, M. Kohda, J. Nitta, and K. Takanashi, Coercivity change in an FePt thin layer in a Hall device by voltage application, Appl. Phys. Lett. **98**, 212505 (2011).

[9] K. Kita, D. W. Abraham, M. J. Gajek, and D. C. Worledge, Electric-field-control of magnetic anisotropy of $\mathrm{Co_{0.6}Fe_{0.2}B_{0.2}}$/oxide stacks using reduced voltage, J. Appl. Phys. **112**, 033919 (2012).

[10] T. Nozaki, Y. Shiota, M. Shiraishi, T. Shinjo, and Y. Suzuki, Voltage-induced perpendicular magnetic anisotropy change in magnetic tunnel junctions, Appl. Phys. Lett. **96**, 022506 (2010).

[11] Y. Shiota, S. Murakami, F. Bonell, T. Nozaki, T. Shinjo, and Y. Suzuki, Quantitative evaluation of voltage-induced magnetic anisotropy change by magnetoresistance measurement, Appl. Phys. Express **4**, 043005 (2011).

[12] W. Skowroński, P. Wiśniowski, T. Stobiecki, S. Cardoso, P. P. Freitas, and S. van Dijken, Magnetic field sensor with voltage-tunable sensing properties, Appl. Phys. Lett. **101**, 192401 (2012).

[13] P. Khalili Amiri, P. Upadhyaya, J. G. Alzate, and K. L. Wang, Electric-field-induced thermally assisted switching of monodomain magnetic bits, J. Appl. Phys. **113**, 013912 (2013).

[14] A. Rajanikanth, T. Hauet, F. Montaigne, S. Mangin, and S. Andrieu, Magnetic anisotropy modified by electric field in V/Fe/MgO(001)/Fe epitaxial magnetic tunnel junction, Appl. Phys. Lett. **103**, 062402 (2013).

[15] Y. Shiota, F. Bonell, S. Miwa, N. Mizunouchi, T. Shinjo, and Y. Suzuki, Opposite signs of voltage-induced perpendicular magnetic anisotropy change in CoFeB/MgO junctions with different underlayers, Appl. Phys. Lett. **103**, 082410 (2013).

[16] T. Nozaki, K. Yakushiji, S. Tamaru, M. Sekine, R. Matsumoto, M. Konoto, H. Kubota, A. Fukushima, and S. Yuasa, Voltage-induced magnetic anisotropy changes in an ultrathin FeB layer sandwiched between two MgO layers, Appl. Phys. Express **6**, 073005 (2013).

[17] T. Nozaki, H. Arai, K. Yakushiji, S. Tamaru, H. Kubota, H. Imamura, A. Fukushima, and S. Yuasa, Magnetization switching assisted by high-frequency-voltage-induced ferromagnetic resonance, Appl. Phys. Express **7**, 073002 (2014).

[18] J. G. Alzate, P. Khalili Amiri, G. Yu, P. Upadhyaya, J. A. Katine, J. Langer, B. Ocker, I. N. Krivorotov, and K. L. Wang, Temperature dependence of the voltage-controlled perpendicular anisotropy in nanoscale MgO/CoFeB/Ta magnetic tunnel junctions, Appl. Phys. Lett. **104**, 112410 (2014).

[19] V. B. Naik, H. Meng, J. X. Xiao, R. S. Liu, A. Kumar, K. Y. Zeng, P. Luo, and S. Yap, Effect of electric-field on the perpendicular magnetic anisotropy and strain in CoFeB/MgO magnetic tunnel junctions, Appl. Phys. Lett. **105**, 052403 (2014).

[20] A. Sonntag, J. Hermenau, A. Schlenhoff, J. Friedlein, S. Krause, and R. Wiesendanger, Electric-Field-Induced Magnetic Anisotropy in a Nanomagnet Investigated on the Atomic Scale, Phys. Rev. Lett. **112**, 017204 (2014).

[21] W. Skowroński, T. Nozaki, Y. Shiota, S. Tamaru, K. Yakushiji, H. Kubota, A. Fukushima, S. Yuasa, and Y. Suzuki, Perpendicular magnetic anisotropy of Ir/CoFeB/MgO trilayer system tuned by electric fields, Appl. Phys. Express **8**, 053003 (2015).

[22] W. Skowroński, T. Nozaki, D. D. Lam, Y. Shiota, K. Yakushiji, H. Kubota, A. Fukushima, S. Yuasa, and Y. Suzuki, Underlayer material influence on electric-field controlled perpendicular magnetic anisotropy in CoFeB/MgO magnetic tunnel junctions, Phys. Rev. B **91**, 184410 (2015).

[23] D. Chiba, M. Sawicki, Y. Nishitani, Y. Nakatani, F. Matsukura, and H. Ohno, Magnetization vector manipulation by electric fields, Nature (London) **455**, 515 (2008).

[24] T. Nozaki, Y. Shiota, S. Murakami, F. Bonell, S. Ishibashi, H. Kubota, K. Yakushiji, T. Saruya, A. Fukushima, S. Yuasa, T. Shinjo, and Y. Suzuki, Electric-field-induced ferromagnetic resonance excitation in an ultrathin ferromagnetic metal layer, Nat. Phys. **8**, 491 (2012).

[25] J. Zhu, J. A. Katine, G. E. Rowlands, Y.-J. Chen, Z. Duan, J. G. Alzate, P. Upadhyaya, J. Langer, P. K. Amiri, K. L. Wang, and I. N. Krivorotov, Voltage-Induced Ferromagnetic Resonance in Magnetic Tunnel Junctions, Phys. Rev. Lett. **108**, 197203 (2012).

[26] Y. Shiota, T. Nozaki, F. Bonell, S. Murakami, T. Shinjo, and Y. Suzuki, Induction of coherent magnetization switching in a few atomic layers of FeCo using voltage pulses, Nat. Mater. **11**, 39 (2012).

[27] S. Kanai, M. Yamanouchi, S. Ikeda, Y. Nakatani, F. Matsukura, and H. Ohno, Electric-field-induced magnetization reversal in a perpendicular-anisotropy CoFeB-MgO magnetic tunnel junction, Appl. Phys. Lett. **101**, 122403 (2012).

[28] W.-G. Wang, M. Li, S. Hageman, and C. L. Chien, Electric-field-assisted switching in magnetic tunnel junctions, Nat. Mater. **11**, 64 (2012).

[29] S. Kanai, Y. Nakatani, M. Yamanouchi, S. Ikeda, H. Sato, F. Matsukura, and H. Ohno, Magnetization switching in a CoFeB/MgO magnetic tunnel junction by combining spin-transfer torque and electric field-effect, Appl. Phys. Lett. **104**, 212406 (2014).

[30] C.-G. Duan, J. P. Velev, R. F. Sabirianov, Z. Zhu, J. Chu, S. S. Jaswal, and E. Y. Tsymbal, Surface Magnetoelectric Effect in Ferromagnetic Metal Films, Phys. Rev. Lett. **101**, 137201 (2008).

[31] K. Nakamura, R. Shimabukuro, Y. Fujiwara, T. Akiyama, T. Ito, and A. J. Freeman, Giant Modification of the Magnetocrystalline Anisotropy in Transition-Metal Monolayers by an External Electric Field, Phys. Rev. Lett. **102**, 187201 (2009).

[32] M. Tsujikawa and T. Oda, Finite Electric Field Effects in the Large Perpendicular Magnetic Anisotropy Surface Pt/Fe/Pt(001): A First-Principles Study, Phys. Rev. Lett. **102**, 247203 (2009).

[33] U. Bauer, L. Yao, A. J. Tan, P. Agrawal, S. Emori, H. L. Tuller, S. van Dijken, and G. S. D. Beach, Magneto-ionic control of interfacial magnetism, Nat. Mater. **14**, 174 (2015).

[34] F. Bonell, Y. T. Takahashi, D. D. Lam, S. Yoshida, Y. Shiota, S. Miwa, T. Nakamura, and Y. Suzuki, Reversible change in the oxidation state and magnetic circular dichroism of Fe driven by an electric field at the FeCo/MgO interface, Appl. Phys. Lett. **102**, 152401 (2013).

[35] L. Xu and S. Zhang, Electric field control of interface magnetic anisotropy, J. Appl. Phys. **111**, 07C501 (2012).

[36] S. E. Barnes, J. Ieda, and S. Maekawa, Rashba spin-orbit anisotropy and the electric field control of magnetism, Sci. Rep. **4**, 4105 (2013).

[37] U. Bauer, M. Przybylski, J. Kirschner, and G. S. D. Beach, Magnetoelectric charge trap memory, Nano Lett. **12**, 1437 (2012).

[38] S. Yuasa, A. Fukushima, K. Yakushiji, T. Nozaki, M. Konoto, H. Maehara, H. Kubota, T. Taniguchi, H. Arai, H. Imamura, K. Ando, Y. Shiota, F. Bonell, Y. Suzuki, N. Shimomura, E. Kitagawa, J. Ito, S. Fujita, K. Abe, K. Nomura, H. Noguchi, and H. Yoda, Future prospects of MRAM technologies, in *Electron Devices Meeting (IEDM), 2013 IEEE International, Washington, DC, 2013* (IEEE, 2013), p. 3.1.1.

[39] Y. Shiota, T. Nozaki, S. Tamaru, K. Yakushiji, H. Kubota, A. Fukushima, S. Yuasa, and Y. Suzuki, Evaluation of

write error rate for voltage-driven dynamic magnetization switching in magnetic tunnel junctions with perpendicular magnetization, Appl. Phys. Express **9**, 013001 (2016).

[40] C.-H. Lambert, A. Rajanikanth, T. Hauet, S. Mangin, E. E. Fullerton, and S. Andrieu, Quantifying perpendicular magnetic anisotropy at the Fe-MgO(001) interface, Appl. Phys. Lett. **102**, 122410 (2013).

[41] J. W. Koo, S. Mitani, T. T. Sasaki, H. Sukegawa, Z. C. Wen, T. Ohkubo, T. Niizeki, K. Inomata, and K. Hono, Large perpendicular magnetic anisotropy at Fe/MgO interface, Appl. Phys. Lett. **103**, 192401 (2013).

[42] F. Bonell, D. D. Lam, S. Yoshida, T. Takahashi, Y. Shiota, S. Miwa, T. Nakamura, and Y. Suzuki, Investigation of Au and Ag segregation on Fe(001) with soft x-ray absorption, Surf. Sci. **616**, 125 (2013).

[43] H. Oka, A. Nakai, and K. Sueoka, Carbon-induced superstructure on Cr(001) thin-film surfaces, Jpn. J. Appl. Phys. **46**, 5602 (2007).

[44] U. Gradmann and J. Mueller, Flat ferromagnetic, epitaxial 48Ni/52Fe(111) films of few atomic layers, Phys. Status Solidi **27**, 313 (1968).

[45] R. Shimabukuro, K. Nakamura, T. Akiyama, and T. Ito, Electric field effects on magnetocrystalline anisotropy in ferromagnetic Fe monolayers, Physica (Amsterdam) **42E**, 1014 (2010).

[46] H. X. Yang, M. Chshiev, B. Dieny, J. H. Lee, A. Manchon, and K. H. Shin, First-principles investigation of the very large perpendicular magnetic anisotropy at Fe/MgO and Co/MgO interfaces, Phys. Rev. B **84**, 054401 (2011).

[47] J. Okabayashi, J. W. Koo, H. Sukegawa, S. Mitani, Y. Takagi, and T. Yokoyama, Perpendicular magnetic anisotropy at the interface between ultrathin Fe and MgO studied by angular-dependent x-ray magnetic circular dichroism, Appl. Phys. Lett. **105**, 122408 (2014).

[48] R. Zhang and R. F. Willis, Thickness-Dependent Curie Temperatures of Ultrathin Magnetic Films: Effect of the Range of Spin-Spin Interactions, Phys. Rev. Lett. **86**, 2665 (2001).

[49] F. J. A. den Broeder, W. Hoving, and P. J. H. Bloemen, Magnetic anisotropy of multilayers, J. Magn. Magn. Mater. **93**, 562 (1991).

[50] A. J. Schellekens, A. van den Brink, J. H. Franken, H. J. M. Swagten, and B. Koopmans, Electric-field control of domain wall motion in perpendicularly magnetized materials, Nat. Commun. **3**, 847 (2012).

[51] D. Chiba, M. Kawaguchi, S. Fukami, N. Ishiwata, K. Shimamura, K. Kobayashi, and T. Ono, Electric-field control of magnetic domain-wall velocity in ultrathin cobalt with perpendicular magnetization, Nat. Commun. **3**, 888 (2012).

[52] S. Emori, U. Bauer, S. Woo, and G. S. D. Beach, Large voltage-induced modification of spin-orbit torques in Pt/Co/GdOx, Appl. Phys. Lett. **105**, 222401 (2014).

[53] H.-M. Benia, P. Myrach, A. Gonchar, T. Risse, N. Nilius, and H.-J. Freund, Electron trapping in misfit dislocations of MgO thin films, Phys. Rev. B **81**, 241415(R) (2010).

[54] S. A. Dababi, R. C. Sousa, M. Chishiev, H. Bea, J. A. Herault, L. Lombard, I. L. Prejbeanu, K. Mackay, and B. Dieny, Charge trapping-detrapping mechanism of barrier breakdown in MgO magnetic tunnel junctions, Appl. Phys. Lett. **99**, 083501 (2011).

[55] S. Miwa, K. Matsuda, K. Tanaka, Y. Kotani, M. Goto, T. Nakamura, and Y. Suzuki, Voltage-controlled magnetic anisotropy in Fe/MgO tunnel junctions studied by x-ray absorption spectroscopy, Appl. Phys. Lett. **107**, 162402 (2015).

[56] P.-J. Zermatten, G. Gaudin, G. Maris, M. Miron, A. Schuhl, C. Tiusan, F. Greullet, and M. Hehn, Experimental evidence of interface resonance states in single-crystal magnetic tunnel junctions, Phys. Rev. B **78**, 033301 (2008).

[57] D. Yoshikawa, M. Obata, Y. Taguchi, S. Haraguchi, and T. Oda, Possible origin of nonlinear magnetic anisotropy variation in electric field effect in a double interface system, Appl. Phys. Express **7**, 113005 (2014).

[58] A. Davies, J. A. Stroscio, D. T. Pierce, and R. J. Celotta, Atomic-Scale Observation of Alloying at the Cr-Fe(001) Interface, Phys. Rev. Lett. **76**, 4175 (1996).

[59] Y. J. Choi, I. C. Jeong, J.-Y. Park, S.-J. Kahng, J. Lee, and Y. Kuk, Surface alloy formation of Fe on Cr(100) studied by scanning tunneling microscopy, Phys. Rev. B **59**, 10918 (1999).

[60] P. V. Ong, N. Kioussis, D. Odkhuu, P. Khalili Amiri, K. L. Wang, and G. P. Carman, Giant voltage modulation of magnetic anisotropy in strained heavy metal/magnet/insulator heterostructures, Phys. Rev. B **92**, 020407(R) (2015).